Article

Measurement and Analysis on Magnetic Field Influence of Substation for Magnetic Shielding Device

Yuan Cheng [1,2], Yaozhi Luo [1], Ruihong Shen [1,2,*], Liang Zhao [2] and Weiyong Zhou [3]

[1] College of Civil Engineering and Architecture, Zhejiang University, Hangzhou 310052, China
[2] China United Engineering Co., Ltd., Hangzhou 310052, China
[3] School of Instrumentation Science and Optoelectronics Engineering, Beihang University, Beijing 100191, China
* Correspondence: srh_1023@163.com

Abstract: The residual magnetic field in a magnetic shielding device with a multilayer high permeability material (permalloy) structure can be obtained at the nanotesla (nT) level or even lower. At present, in the process of designing a magnetic shielding device, most of the external environmental magnetic field settings are set at the size of the Earth's environmental magnetic field, but the instruments inside the magnetic shielding device need to be powered, the active compensation coil needs to be powered, and the degaussing coil of passive shielding layer needs to be powered, so substations need to be used around magnetic shielding devices. The magnetic field generated by the substation will affect the magnetic shielding device, so this paper analyzes and measures the magnetic field generated by the substation. Firstly, the finite element model of a substation is established, and the influence of different substations on the environmental magnetic field is analyzed by changing the power. Secondly, the test method of a substation environment magnetic field is determined. Finally, the site test was carried out to measure the influence of different power substations and different distances on the magnetic field, and its influence on the magnetic shielding device was analyzed, which provided an important basis for the construction of the magnetic shielding device.

Keywords: magnetic shielding device; extremely weak magnetic field; substation

1. Introduction

A magnetic shielding device shields low-frequency and static magnetic fields through the flux shunt effect [1–3] of high permeability magnetic materials (such as permalloy), shields AC magnetic fields through the eddy current effect [4,5] of high conductivity materials (such as aluminum and copper), and prevents external magnetic fields from entering its interior through shielding, thus, generating an extremely weak magnetic field environment inside. In the weak magnetic environment, many scholars carried out frontier work, such as measuring biological signals such as in the heart and brain [6–8], measuring geophysical research samples [9], measuring electric dipole moments [10], and researching high-precision magnetic measurement instruments, such as SERF atomic gyroscopes and magnetometers [11,12]. As the internal magnetic field of a magnetic shielding device is very weak, the magnetic shielding device system is vulnerable to the interference of a strong external magnetic field. In order to achieve better shielding effect, a magnetic shielding device is usually equipped with an active compensation coil outside to provide active magnetic field shielding, the passive shielding layer needs demagnetization, and the internal experimental instruments need power supply. All the above need to be equipped with substations for power supply, which may affect the shielding performance of magnetic shielding devices.

For the research of magnetic shielding devices, many scholars use active compensation coils to improve the uniformity of the residual magnetic field inside the magnetic shielding device [13–15]. Altarev et al. [16] reported a degaussing method for a magnetic shielding

device, which can shorten the degaussing time by 10 times, significantly reduce the residual magnetic field of magnetic shielding devices, and improve the uniformity. Therefore, it is of great significance to study the influence of the substation used by magnetic shielding devices on the surrounding magnetic field for the positioning and design of the magnetic shielding device.

In view of the influence of substations and other electrical equipment on the environmental magnetic field, many scholars carried out relevant research work [17–30]. Some scholars introduced finite element simulation into the analysis of electric and magnetic fields generated by substations: Zhou et al. [17] used the finite element method to analyze the power frequency magnetic field distribution characteristics of a typical 2 × 80 MVA substation. The results showed that the maximum magnetic induction intensity of 15 m around the substation was less than 1.6 μT. For the electromagnetic environment of a 500 kV substation, Chen et al. [18] proposed a full-scale simulation model using boundary element method (BEM) to calculate the distribution of the electric and magnetic fields, and obtained the distribution of electric and magnetic fields in the substation. Sakai et al. [19] studied the extremely low frequency (ELF) magnetic field environment distribution of a 500 kV/ 275 kV gas-insulated substation by comparing the measurement results with the finite element method (FEM) calculation results. Hosseinabadi et al. [20] measured the influence of different units of a thermal power plant on the surrounding magnetic field and simulated it through ArcGIS software v. 10.7.1. The exposure effect is ranked according to the size of the magnetic field, but the actual measured value is higher than the simulation value, so the simulation method needs to be further improved. Medved et al. [21] analyzed the solution method of electromagnetic field distribution in a 110 kV substation, and simulated it in ANSYS, solving the distribution of electric field and magnetic field. Three positions with different heights from the ground are selected for measurement, and the measurement results are compared with the simulation results with good consistency. Carlos et al. [22] designed a software to calculate the magnetic field near electrical equipment based on low-frequency Maxwell equations, which can be used to calculate and express three-dimensionally the magnetic field generated by current circulation in electrical facilities.

Some scholars studied the occupational exposure caused by electric and magnetic fields generated by substations: Pirkkalainen et al. [23] tested the power plants around the 220 KV substation and determined the scope of work less than the occupational exposure standard. Yang et al. [24] measured the magnetic induction intensity of the reactor under the full load operational condition of a ±660 kV substation. According to the magnetic field distribution, they proposed a method to eliminate the influence of the Earth's magnetic field by combining the measured data. Fontgalland et al. [25] estimated the electric field and magnetic field of a 400 MVA substation through measurement and interpolation, and drew a two-dimensional contour map. Qiu et al. [26] tested the power frequency magnetic field data of a 10 KV substation, analyzed the test data, and gave the overall distribution characteristics of the power frequency magnetic field of the substation. Okrainskaya et al. [27] tested the magnetic field intensity distribution of a 500 kV power substation and analyzed the impact of various devices in the substation on the environmental magnetic field. Hosseinabadi et al. and Liu et al. [28] studied the magnetic field distribution around a 10 kV switchgear and the shielding efficiency of the enclosure. The mathematical model of the power frequency magnetic field of the switchgear is established, and the magnetic induction intensity is solved by using the finite element method. The results show that when the distance from the switchgear door is less than 0.6 m, the magnetic induction intensity can reach the public exposure limit of 100μT. Tognola et al. [29] analyzed and compared children living near high voltage (63–150 kV), ultra-high voltage (225 kV), and ultra-high voltage (400 kV) overhead lines with children living near low-voltage (400 V), medium voltage (20 kV), and substation (20 kV/400 V) underground networks. They found that the former had higher exposure levels, which proved that high-voltage lines had a greater impact on magnetic fields. Frigura-Iliasa et al. [30] tested the root mean square (RMS) values of a low-frequency (0–300 Hz) electric field strength and magnetic flux density of different parts of the high-voltage power

station in different time periods, and determined the working place and safe exposure time of the operators.

In previous studies, scholars mainly studied the occupational exposure caused by electric and magnetic fields generated by substations and did not analyze the possible impact of substations on magnetic shielding devices. In order to evaluate the possible influence of the substation with common power of magnetic shielding devices (active compensation coil power supply 323 kW, degaussing power supply 1630 kW, internal equipment power supply 9 kW) on the magnetic shielding device due to the nearby space magnetic field, this paper establishes a finite element model, conducts magnetic field simulation, and analyzes the magnetic field influence range of the above power substations through a field test of the space DC magnetic field and AC magnetic field fluctuation data of substations at different distances. It provides a basis for the site selection and design of magnetic shielding device substations.

2. FEM Results of Substation Magnetic Field Influence

The magnetic shielding device usually consists of a passive shielding layer, an active compensation coil, and a degaussing coil. The passive shielding layer mostly uses soft magnetic materials such as permalloy to shield the magnetic field through the principle of flux diversion. The active compensation coil generates a magnetic field opposite to the Earth's magnetic field through Biot–Savart's law to offset the magnetic field. The degaussing coil is arranged on the passive magnetic shielding layer, the magnetic field generated by Biot–Savart's law makes the passive magnetic shielding reach the magnetic saturation state, gradually reduces the magnetic field, and reduces the influence of factors such as the stress of the passive magnetic shielding layer during installation on the shielding performance. The experiment was carried out in the internal extremely weak magnetic field space. Common measuring instruments include SERF atomic magnetometer, SERF atomic gyroscope, electric dipole moment test system, and so on. The structure is shown in Figure 1. Due to different applications, active compensation coils, degaussing coils, and instruments need power supplies with different power requirements, among which, the active compensation coils need long-term operation and stable power supplies, the degaussing coils need power supplies with high power and fast response, and the instruments need less power. Therefore, magnetic field analysis is conducted for 323 kW (active compensation coil), 1630 kW (degaussing coil), and 9 kW (instrument) substations according to different power demands.
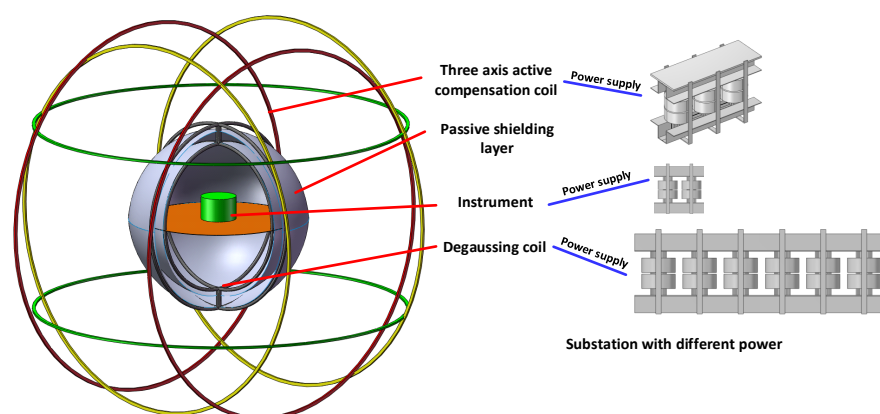

Figure 1. Schematic diagram of magnetic shielding device.

Through the finite element simulation software COMSOL, the finite element model of a substation is established, including primary coil, secondary coil, and iron core. The magnetic field generated by 323 kW, 1630 kW, and 9 kW substations is simulated by finite element method by changing the current and other parameters (the number of elements s is 58,000 (substation 1), 76,000 (substation 2), 27,000 (substation 3), and the current is 415 A

(substation 1), 3000 A (substation 2), and 15 A (substation 3), and the impact of different substations on the environmental magnetic field is analyzed. The three substations have the same type and use the same model for calculation. The current in the substation is modified by modifying the current value of the primary coil. The simulation results are shown in Figure 2, the unit of magnetic field is nT.
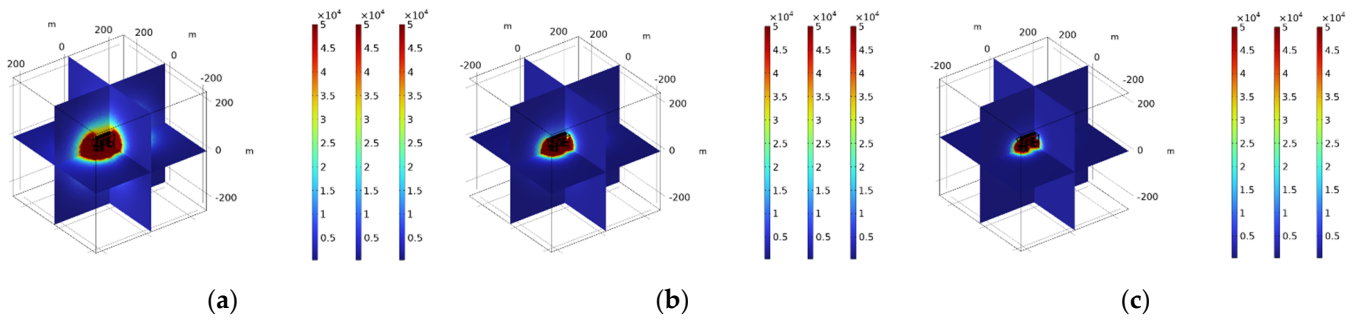

Figure 2. Simulation results of substation environmental magnetic field (the color scale on the right side of the figure represents the magnetic induction intensity). (**a**) Substation 1 (323 kW); (**b**) substation 2 (1630 kW); (**c**) substation 3 (9 kW).

According to the simulation results, the influence range of the magnetic field generated by the substation is analyzed. The magnetic field section is drawn through the 3D drawing group, and the magnetic field distribution is obtained. The magnetic field of the substation weakens at different speeds in different directions. In order to ensure that the magnetic field attenuates to a safe size under a certain radius, the radius is determined according to the maximum magnetic field value (to ensure that the maximum magnetic field value under the radius is less than the Earth's magnetic field). According to the analysis results, for substation 1 (323 kW), the magnetic field can be attenuated to a level close to the Earth's magnetic field (about 50,000 nT) beyond the radius of 15 m around the substation. For substation 2 (1630 kW), the magnetic field can be attenuated to a level close to the Earth's magnetic field beyond the radius of 60 m around the substation. For substation 3 (9 kW), the magnetic field can be attenuated to a level close to the Earth's magnetic field beyond the radius of 5 m around the substation. As shown in Figure 3, this result proves that the substation has an impact on the environmental magnetic field, and the impact attenuates with the increase in distance. Therefore, the construction of a magnetic shielding device must maintain a safe distance from its supporting substation.
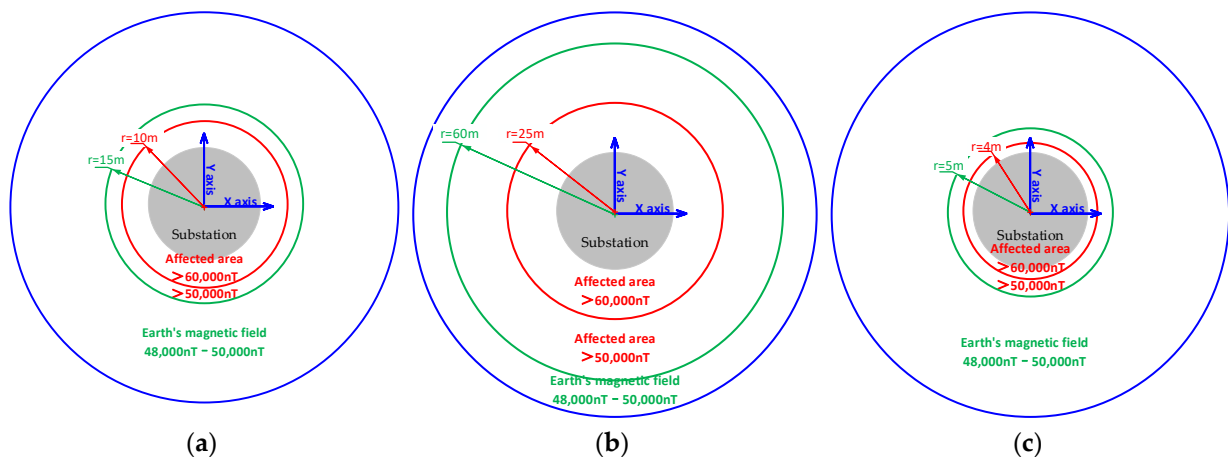

Figure 3. Influence range of substation environmental magnetic field. (**a**) Substation 1; (**b**) substation 2; (**c**) substation 3.

3. Principle of Measurement

Shielding factor of magnetic shielding device can be calculated as follows (single-layer shielding cylinder) [31]:

$$S_s = \frac{2\mu t R^{\frac{1}{2}}}{L^{\frac{3}{2}}} \tag{1}$$

where S_s is the single-layer shielding factor; μ is the relative permeability; R is the radius of the shielding layer; t is the thickness of the shielding layer; L is the length of the shielding layer.

The formula for calculating the shielding factor of the multi-layer magnetic shielding cylinder is:

$$S_z = S_n \prod_{i=1}^{n-1} S_i \left[1 - \left(\frac{D_{i+1}}{D_i} \right)^j \right] \tag{2}$$

where S_z is the n-layer radial shielding coefficient; S_i is the i-th layer shielding coefficient (the outermost is the first layer).

The remanence of the magnetic shielding device B can be calculated by the magnetic shielding factor S_z:

$$B = \frac{B_0}{S_z} \tag{3}$$

where B_0 is the background magnetic field.

According to the above formula, when the material permeability, size, and other parameters of the magnetic shielding device are determined, the background magnetic field strength is an important factor affecting the internal remanence of the magnetic shielding device.

The environmental magnetic field is tested by a three-axis fluxgate magnetometer, where B_X is the east–west magnetic field (facing west is positive), B_Y is the vertical to the ground magnetic field (facing the ground is positive), B_Z is the north–south magnetic field (facing north is positive), and B_T is the total magnetic field:

$$B_T = \sqrt{B_x^2 + B_y^2 + B_z^2} \tag{4}$$

Follow the test steps:

(1) Determine the test distance, take the substation to be tested as the center, and use a tape measure to determine the test point;
(2) Set the three-axis fluxgate at the test point through the tooling;
(3) Turn on the three-axis flux gate to preheat for 10 min, and open the acquisition board and computer;
(4) Read and store test data through computer;
(5) Calculate the magnetic field with Formula (4);
(6) Repeat (1)–(5) to test the next test point.

Use a tripod to fix the fluxgate magnetometer and its clamp, as shown in Figure 4. Use a tape measure to measure the distance from the test point to the measured substation, and test according to the above steps.
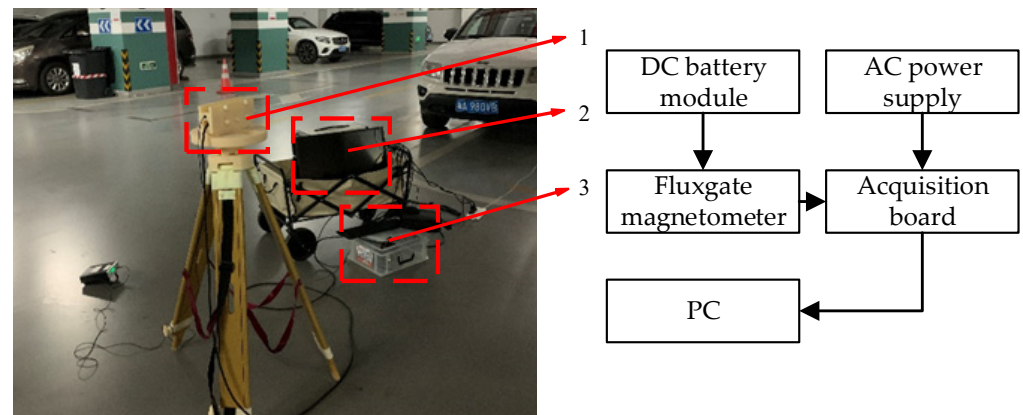
Figure 4. Image of testing device: (1) fluxgate magnetometer probe, (2) PC, (3) acquisition board.

4. Test Results and Discussion

According to the above test principles and test steps, magnetic field tests were carried out for different types of substations to be used in magnetic shielding devices. It included 323 kW substation 1 (intended for active compensation coil), 1630 kW substation 2 (intended for degaussing coil), and 9 kW substation 3 (intended for instrument). According to the internal use demand of the magnetic shielding device, the indicators for evaluating the shielding effect of the magnetic shielding device include the DC residual magnetic field value and magnetic field fluctuation, so the test includes the static magnetic field value and magnetic field fluctuation value at different distances. The magnetic field of the same day at different times and at the same location on different days is tested, and the results show that the difference is very small, so a test result on the same day is given. According to the simulation analysis in Figure 2, the magnetic field of the substation weakens at different speeds in different directions, so the magnetic field in four directions (east, west, north, and south) was tested and the maximum direction of the magnetic field was taken as the basis for judging the distance.

4.1. Magnetic Field near Substation 1

Substation 1 is intended to provide power for the active compensation coil. The working state of substation 1 tested is 323 kW power and 415 A current. The height of the measuring support from the ground is 1.1 m. The site photos are shown in Figure 5:
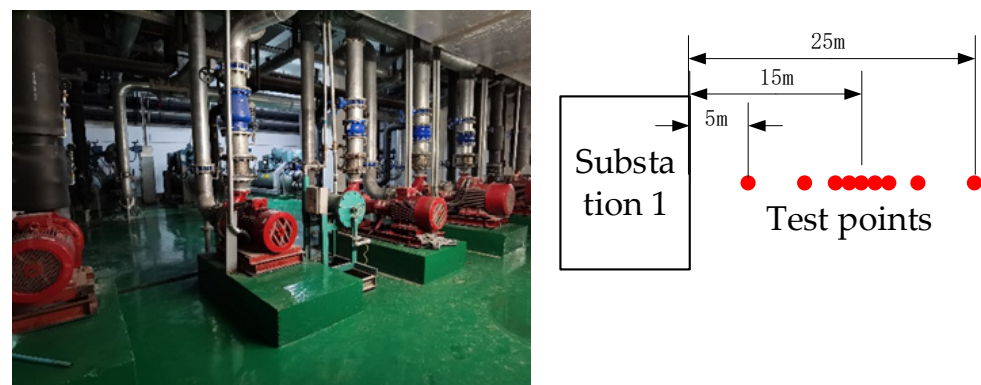

Figure 5. Image of substation 1.

We take nine test sample points at substation 1, which are from 5 m (test point 1) to 25 m (test point 5) away from the substation working equipment, with a step length of 5 m (more points are selected around the critical point for testing). The test data are high-frequency filtered through the LabVIEW program, and the test results of the DC magnetic field are shown in Figure 6.
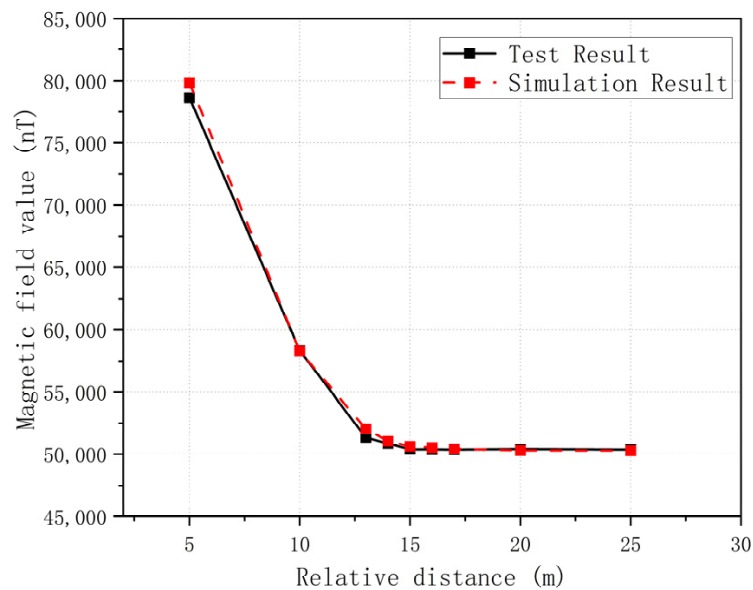
Figure 6. DC magnetic field test results of substation 1.

According to the test results, substation 1 at test point 1 has a large impact on the DC magnetic field, which is about 1.6 times that of the Earth's magnetic field. When the distance between the test point and the substation increases, the magnetic field gradually decreases, and at about 15 m (point 5), decays to the Earth's magnetic field level. In the simulation calculation, the geomagnetic field value obtained from the actual test is added through the "background field" function of the finite element simulation software, and the test results are similar to the simulation results.

At the same time, in order to obtain the influence of magnetic field fluctuation, the Mag-03 magnetic flux gate (noise lower than 6 ptrms/hz$^{1/2}$@1 Hz; the bandwidth is up to 3 kHz (−3 dB), and the measurement accuracy is less than 0.1 nT) is used to collect and record the real magnetic field before filtering (the sampling frequency is 1000 Hz), and a spectrum diagram is drawn (according to the sampling law, the frequency of concern is less than 500 Hz, and in order to obtain effective data and avoid clutter interference, the spectrum diagram is processed at an average of 1 Hz). Figure 7 shows the spectrum analysis diagrams of the east–west, north–south, and vertical to the ground magnetic fields of test point 1. Figure 8 shows the spectrum analysis of the three-axis magnetic field at test point 3.

According to Figure 7, it can be found that the magnetic field near the power frequency (50 Hz) of test point 1 of substation 1 is large and has an impact on multiple frequency bands. The source of non-50 Hz harmonic peak is the multiple frequency interference of 50 Hz, which may be due to the nonlinear load (demagnetization coil and active compensation coil of magnetic shielding device) in the substation, is the main cause of harmonic generation, and the harmonic current generated by the substation causes the multiple frequency interference of magnetic field fluctuations. According to Figure 8, it can be found that the impact of power frequency and other frequency bands is reduced at three test points 15 m away. The maximum amplitude in the magnetic field spectrum of each direction of the test point and frequency corresponding to the maximum amplitude in the test frequency band are listed in Table 1.
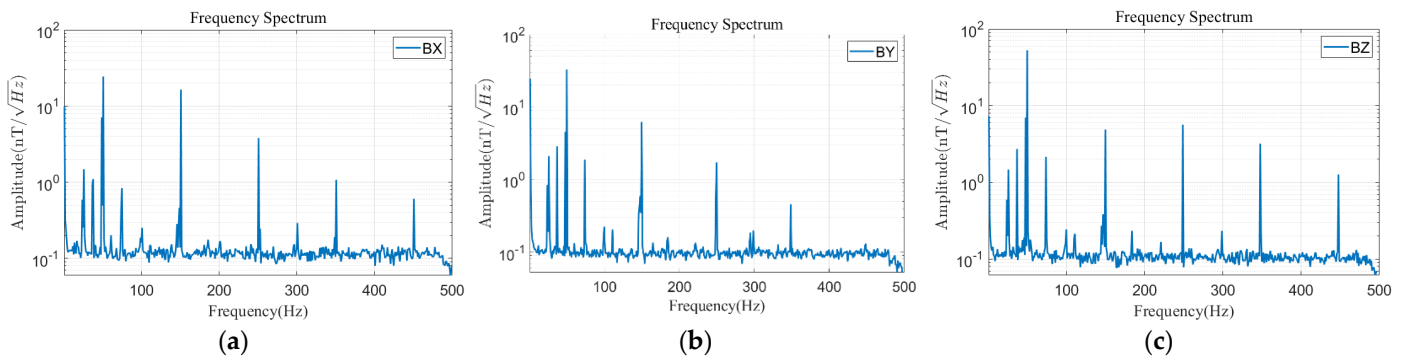
Figure 7. Magnetic field spectrum diagram of test point 1. (**a**) B_X point; (**b**) B_Y point; (**c**) B_Z point.
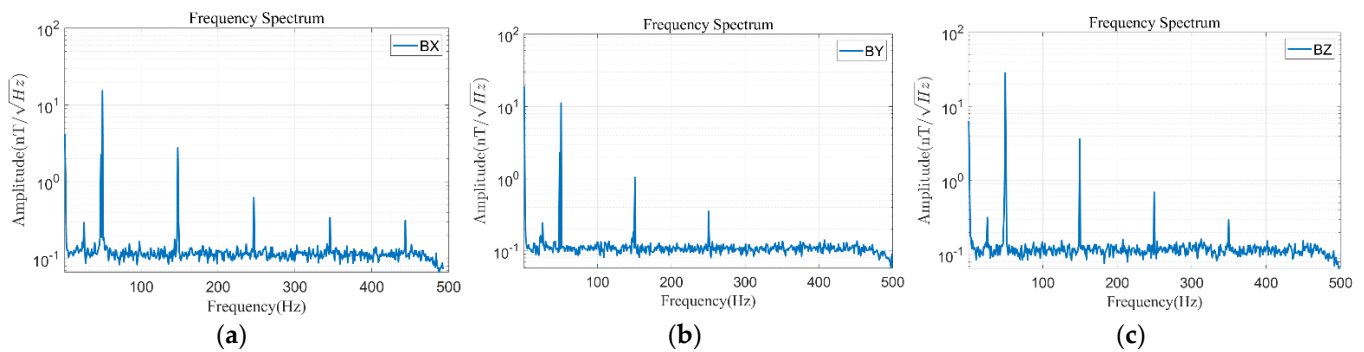

Figure 8. Magnetic field spectrum diagram of test point 3. (**a**) B_X point; (**b**) B_Y point; (**c**) B_Z point.

Table 1. Magnetic field spectrum analysis results of substation 1.

Test Point	B_X (East–West)		B_Y (Vertical to the Ground)		B_Z (North–South)	
	Maximum Amplitude (nT/Hz$^{1/2}$)	Frequency (Hz)	Maximum Amplitude (nT/Hz$^{1/2}$)	Frequency (Hz)	Maximum Amplitude (nT/Hz$^{1/2}$)	Frequency (Hz)
Test point 1 (5 m)	32.5	50	35.7	49.5	38.4	50.5
Test point 5 (15 m)	11.2	49.5	15.4	49.5	20.5	49.5

According to the spectrum data, the magnetic field generated by substation 1 is mainly the power frequency magnetic field. When the test point is 15 m away from the substation, the magnetic field fluctuation is reduced by about 70%. Based on the analysis of DC magnetic field and fluctuating magnetic field, when substation 1 is used, the construction site of the magnetic shielding device should be at least 15 m away from the radius of substation 1.

4.2. Magnetic Field near Substation 2

Substation 2 is designed to supply power to the degaussing coils. The working state of the tested substation 2 is 1630 kW. The height of the measuring support from the ground is 1.1 m. The site photos are shown in Figure 9:

We take eleven test sample points at substation 2, which are from 10 m (test point 1) to 70 m (test point 7) away from the substation working equipment, with a step length of 10 m (more points are selected around the critical point for testing). The remanence test results after high-frequency filtering are shown in Figure 10 (DC data of magnetic field):
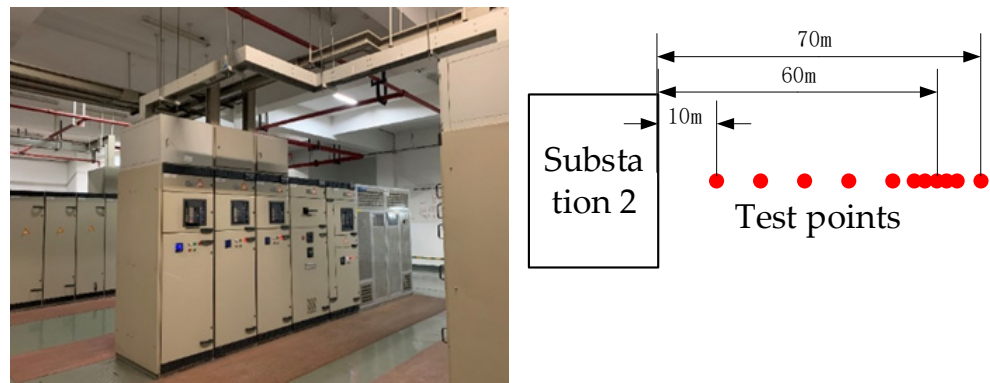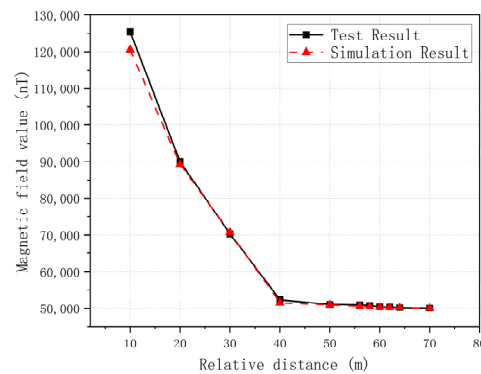
Figure 9. Image of substation 2.

Figure 10. DC magnetic field test results of substation 2.

According to the test results, substation 2 at test point 1 has a large impact on the DC magnetic field, which is about 2.4 times that of the Earth's magnetic field. When the distance between the test point and the substation increases, the magnetic field gradually decreases, and at about 60 m (point 8) decays to the Earth's magnetic field level, which is similar to the simulation results.

Similarly, in order to obtain the influence of magnetic field fluctuation, the Mag-03 fluxgate is used to collect and record the real magnetic field before filtering (the sampling frequency is 1000 Hz), and the spectrum diagram is drawn. Figure 11 shows the spectrum analysis diagrams of the east–west, north–south, and vertical to the ground magnetic fields of test point 1. Figure 12 show the spectrum analysis of the three-axis magnetic field at test point 6.
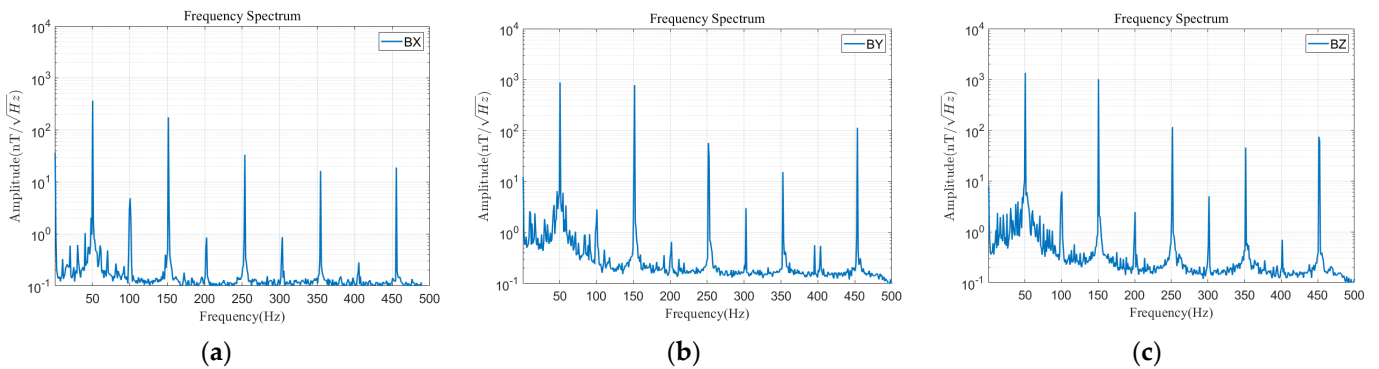

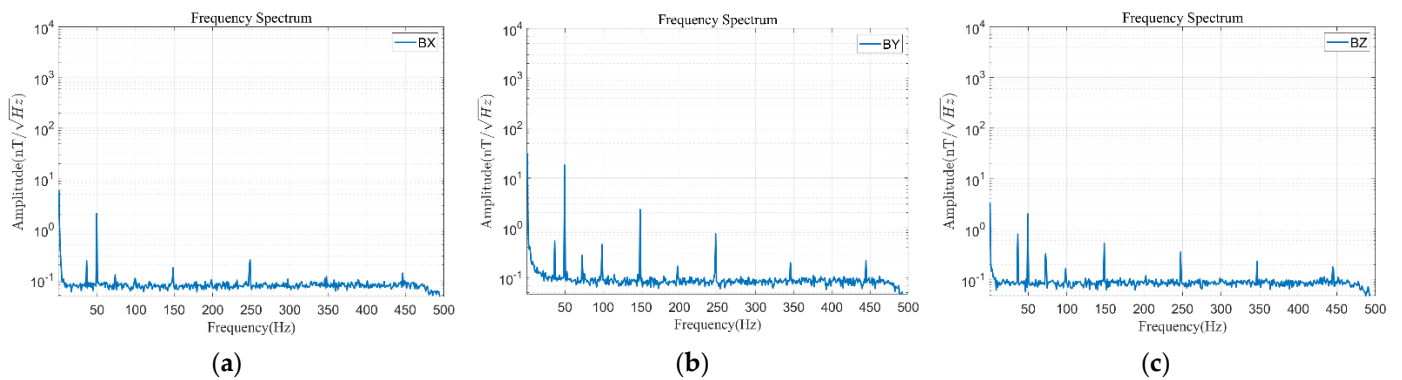**Figure 11.** Magnetic field spectrum diagram of test point 1. (**a**) B_X point; (**b**) B_Y point; (**c**) B_Z point.

Figure 12. Magnetic field spectrum diagram of test point 8. (**a**) B_X point; (**b**) B_Y point; (**c**) B_Z point.

According to Figure 11, it can be found that the magnetic field near the power frequency (50 Hz) of test point 1 of substation 2 is large and has an impact on multiple frequency bands. According to Figure 12, it can be found that the impact of power frequency and other frequency bands is reduced at six test points 60 m away. The maximum amplitude in the magnetic field spectrum of each direction of the test point and frequency corresponding to the maximum amplitude in the test frequency band are listed in Table 2.

Table 2. Magnetic field spectrum analysis results of substation 2.

Test Point	B_X (East–West)		B_Y (Vertical to the Ground)		B_Z (North–South)	
	Maximum Amplitude (nT/Hz$^{1/2}$)	Frequency (Hz)	Maximum Amplitude (nT/Hz$^{1/2}$)	Frequency (Hz)	Maximum Amplitude (nT/Hz$^{1/2}$)	Frequency (Hz)
Test point 1 (10 m)	369.1	49.5	887.0	49.5	1347.0	49.5
Test point 8 (60 m)	12.1	48.5	18.3	48.5	35.3	48.5

According to the spectrum data, the magnetic field generated by substation 2 is mainly power frequency magnetic field. The magnetic field in the power distribution room fluctuates greatly, and the spectrum curve is raised as a whole. The maximum amplitude near 50 Hz can reach 1347.0 nT/Hz$^{1/2}$, indicating that substation 2 has a great impact on the space magnetic field. However, when the test point is 60 m away from the substation, the magnetic field fluctuation is reduced by about 90%. Based on the analysis of DC magnetic field and fluctuating magnetic field, when substation 2 is used, the construction site of the magnetic shielding device should be at least 60 m away from the radius of substation 2.

4.3. Magnetic Field near Substation 3

Substation 3 is designed to provide power together inside the magnetic shielding device. The working state of the tested substation 2 is 9 kW. The height of the measuring support from the ground is 1.1 m. The site photos are shown in Figure 13.
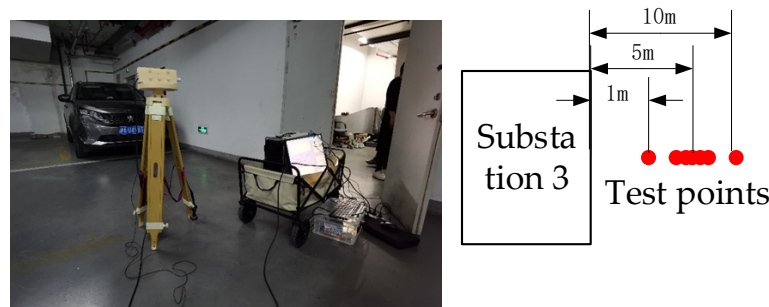

Figure 13. Image of Substation 3.

We take seven test sample points at substation 3, which are 1 m (test point 1) to 10 m (test point 3) away from the substation working equipment, with a step length of about 5 m (more points are selected around the critical point for testing). The remanence test results after high-frequency filtering are shown in Figure 14 (DC data of magnetic field):
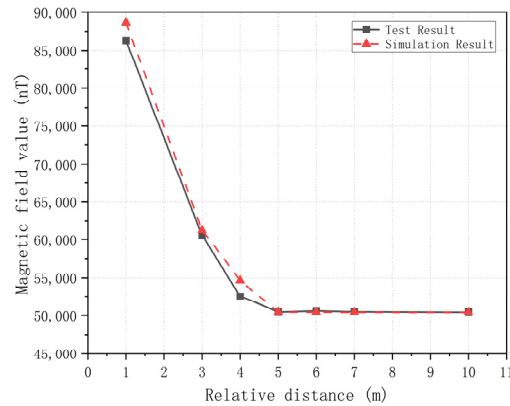

Figure 14. DC magnetic field test results of substation 3.

According to the test results, substation 3 at test point 1 has a large impact on the DC magnetic field, which is about 1.7 times that of the Earth's magnetic field. When the distance between the test point and the substation increases, the magnetic field gradually decreases, and at about 5 m (point 4), decays to the Earth's magnetic field level, which is similar to the simulation results.

Similarly, in order to obtain the magnetic field contribution of each frequency band, the Mag-03 fluxgate is used to collect and record the real magnetic field before filtering (the sampling frequency is 1000 Hz), and the spectrum diagram is drawn. Figure 15 shows the spectrum analysis diagrams of the east–west, north–south, and vertical to the ground magnetic fields of test point 2.
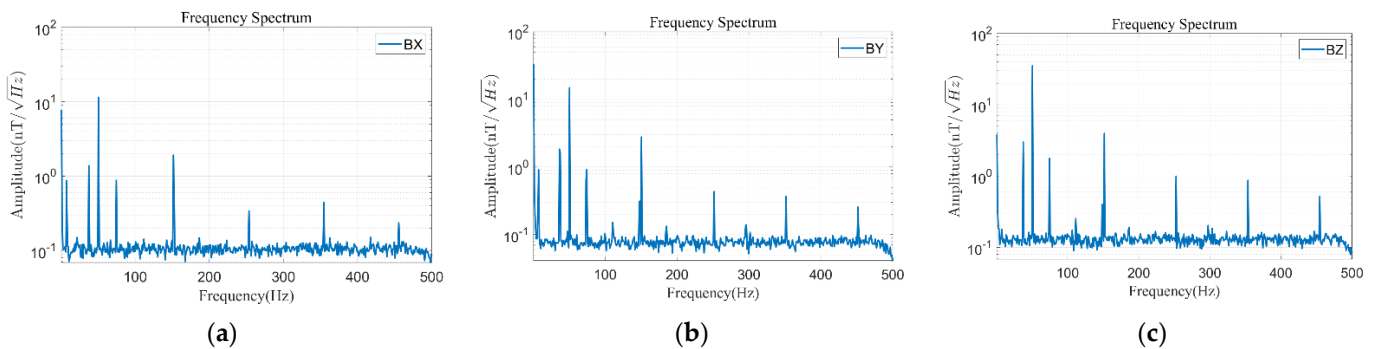

(a) **(b)** **(c)**

Figure 15. Magnetic field spectrum diagram of test point 2. (**a**) B_X point; (**b**) B_Y point; (**c**) B_Z point.

The maximum amplitude in the magnetic field spectrum of each direction of the test point and frequency corresponding to the maximum amplitude in the test frequency band are listed in Table 3.

Table 3. Magnetic field spectrum analysis results of substation 3.

Test Point	B_X (East–West)		B_Y (Vertical to the Ground)		B_Z (North–South)	
	Maximum Amplitude (nT/Hz$^{1/2}$)	Frequency (Hz)	Maximum Amplitude (nT/Hz$^{1/2}$)	Frequency (Hz)	Maximum Amplitude (nT/Hz$^{1/2}$)	Frequency (Hz)
Test point 4	11.9	49.5	14.9	49.5	20.2	49.5

According to the spectrum data, when measured at 5 m from the substation 3, the magnetic field fluctuation approaches the fluctuation level of the Earth's magnetic field. Based on the analysis of DC magnetic field and fluctuating magnetic field, when substation 3 is used, the construction site of magnetic shielding device should be at least 5 m away from the radius of substation 3.

4.4. Discussion

According to the test results, it can be preliminarily concluded that:

(1) The substation has an influence on both the DC and AC magnetic fields, so a certain distance from the substation should be considered when building magnetic shielding devices;

(2) For test point 3 of substation 1 (15 m away from the substation), test point 6 of substation 2 (60 m away from the substation), and test point 2 of substation 3 (5 m away from the substation), the magnetic field attenuates to be equivalent to the Earth's magnetic field and is close to the simulation results. It can be used as the construction site of the magnetic shielding device;

(3) The magnetic field fluctuation caused by the substation also has a great impact on the magnetic shielding device, especially when close to substation 2, the AC magnetic field is large (about two to three orders of magnitude higher), so it is necessary to consider the impact of its working magnetic field on other equipment. After the distance reaches 60 m, the amplitude of the AC magnetic field decreases significantly, which indicates that the safe distance can effectively reduce the influence of the substation magnetic field;

(4) The magnetic field of substations is changed to be based on the magnetic field attenuation of magnetic dipole ($1/d^3$). The formulas of three different substations are analyzed in combination with power, and the general formula including different power is obtained as follows:

$$B = 50,400 + \frac{120\mu_0 \times w}{4\pi * d^3} \times 10^9 \tag{5}$$

where B is the magnetic field strength, d is the shortest distance between the calculation point and the substation, w is the equivalent power, and μ_0 is vacuum permeability, $4\pi \times 10^{-7}$.

5. Conclusions

In order to reduce the influence of substations equipped with magnetic shielding devices on the shielding performance of magnetic shielding devices, the environmental magnetic field near commonly used substations is analyzed through simulation and experimental measurement methods, and its influence on magnetic shielding devices is analyzed. According to the analysis of the test results, the substation has an impact on both DC and AC magnetic fields. When using anything similar to substation 1 (323 kW), the magnetic shielding device should be at least 15 m away from the substation, and when using anything similar to substation 2 (1630 kW), the magnetic shielding device should be at least 60 m away from the substation. Therefore, when using something similar to substation 3 (9 kW), the magnetic shielding device should be at least 5 m away from the substation. The test results are in good agreement with the simulation results. This paper tests the DC magnetic field and magnetic field fluctuation of substations with common power in magnetic shielding devices, and the general formula of substations with different power is obtained for calculating the magnetic field value and distance, which provides a basis for the construction of magnetic shielding devices.

References

1. Li, J.; Quan, W.; Han, B.; Wang, Z.; Fang, J. Design and Optimization of Multilayer Cylindrical Magnetic Shield for SERF Atomic Magnetometer Application. *IEEE Sens. J.* **2020**, *20*, 1793–1800. [CrossRef]
2. Kvitkovic, J.; Patel, S.; Pamidi, S. Magnetic Shielding Characteristics of Hybrid High-Temperature Superconductor/Ferromagnetic Material Multilayer Shields. *IEEE Trans. Appl. Supercond.* **2017**, *27*, 1–5. [CrossRef]
3. Packer, M.; Hobson, P.J.; Davis, A.; Holmes, N.; Leggett, J.; Glover, P.; Hardwicke, N.L.; Brookes, M.J.; Bowtell, R.; Fromhold, T.M. Magnetic Field Design in a Cylindrical High-Permeability Shield: The Combination of Simple Building Blocks and a Genetic Algorithm. *arXiv* **2021**, arXiv:2107.03170. [CrossRef]
4. Ates, K.; Carlak, H.F.; Ozen, S. Dosimetry Analysis of the Magnetic Field of Underground Power Cables and Magnetic Field Mitigation Using an Electromagnetic Shielding Technique. *Int. J. Occup. Saf. Ergon.* **2022**, *28*, 1672–1682. [CrossRef]
5. Matsuzawa, S.; Kojima, T.; Mizuno, K.; Kagawa, K.; Wakamatsu, A. Electromagnetic Simulation of Low-Frequency Magnetic Shielding of a Welded Steel Plate. *IEEE Trans. Electromagn. Compat.* **2021**, *63*, 1896–1903. [CrossRef]
6. Holmes, N.; Leggett, J.; Boto, E.; Roberts, G.; Hill, R.M.; Tierney, T.M.; Shah, V.; Barnes, G.R.; Brookes, M.J.; Bowtell, R. A Bi-Planar Coil System for Nulling Background Magnetic Fields in Scalp Mounted Magnetoencephalography. *Neuroimage* **2018**, *181*, 760–774. [CrossRef]
7. Yang, J.; Zhang, X.; Han, B.; Wang, J.; Wang, L. Design of Biplanar Coils for Degrading Residual Field in Magnetic Shielding Room. *IEEE Trans. Instrum. Meas.* **2021**, *70*, 1–10. [CrossRef]
8. Yang, K.; Wu, D.; Gao, W.; Ni, T.; Zhang, Q.; Zhang, H.; Huang, D. Calibration of SQUID Magnetometers in Multichannel MCG System Based on Bi-Planar Coil. *IEEE Trans. Instrum. Meas.* **2022**, *71*, 1–9. [CrossRef]
9. Afach, S.; Bison, G.; Bodek, K.; Burri, F.; Chowdhuri, Z.; Daum, M.; Fertl, M.; Franke, B.; Grujic, Z.; Helaine, V.; et al. Dynamic Stabilization of the Magnetic Field Surrounding the Neutron Electric Dipole Moment Spectrometer at the Paul Scherrer Institute. *J. Appl. Phys.* **2014**, *116*, 084510. [CrossRef]
10. Kuchler, F.; Babcock, E.; Burghoff, M.; Chupp, T.; Degenkolb, S.; Fan, I.; Fierlinger, P.; Gong, F.; Kraegeloh, E.; Kilian, W.; et al. A New Search for the Atomic EDM of 129Xe at FRM-II. *Hyperfine Interact* **2016**, *237*, 95. [CrossRef]
11. Tashiro, K.; Wakiwaka, H.; Matsumura, K.; Okano, K. Desktop Magnetic Shielding System for the Calibration of High-Sensitivity Magnetometers. *IEEE Trans. Magn.* **2011**, *47*, 4270–4273. [CrossRef]
12. Packer, M.; Hobson, P.J.; Holmes, N.; Leggett, J.; Glover, P.; Brookes, M.J.; Bowtell, R.; Fromhold, T.M. Optimal Inverse Design of Magnetic Field Profiles in a Magnetically Shielded Cylinder. *Phys. Rev. Appl.* **2020**, *14*, 054004. [CrossRef]
13. Jin, Y.X.; Li, L.Y.; Pan, D.H.; Song, K.; Lou, S.F.; Zou, Z.L.; Sun, Z.Y. Analysis and Design of a Uniform Magnetic Field Coil With a Magnetic Shield Based on an Improved Analytical Model. *IEEE Trans. Ind. Electron.* **2022**, *69*, 3068–3077. [CrossRef]
14. Fan, W.F.; Quan, W.; Liu, F.; Pang, H.Y.; Xing, L.; Liu, G. Performance of Low-Noise Ferrite Shield in a K-Rb-Ne-21 Co-Magnetometer. *IEEE Sens. J.* **2020**, *20*, 2543–2549. [CrossRef]
15. Pan, D.H.; Lin, S.X.; Li, L.Y.; Li, J.; Jin, Y.X.; Sun, Z.Y.; Liu, T.H. Research on the Design Method of Uniform Magnetic Field Coil Based on the MSR. *IEEE Trans. Ind. Electron.* **2020**, *67*, 1348–1356. [CrossRef]
16. Altarev, I.; Fierlinger, P.; Lins, T. Minimizing magnetic fields for precision experiments. *J. Appl. Phys.* **2015**, *117*, 233903-1–233903-5. [CrossRef]
17. Zhou, K.; Jin, Q.R.; Wang, X.M.; Peng, B.; Sun, H.D. Auxiliary simulation analysis of micro intelligent sensor for power frequency magnetic field distribution characteristics of typical substation. In Proceedings of the 2nd International Conference for Information Systems and Design (ICID), Xi'an, China, 3–7 September 2021; pp. 273–277.
18. Chen, Y.D.; Wang, F.S.; Li, T.Y.; Tang, K.D.; Fang, Z.K.; Ye, M. Research on electromagnetic environment characteristics of 500 kV full-scale substation based on BEM. In Proceedings of the 2nd International Conference on Energy Engineering and Environmental Protection (EEEP), Sanya, China, 20–22 November 2017.
19. Sakai, K.; Kato, K.; Okubo, H.; Matsumoto, A. ELF magnetic field measurement and calculation in 500 kV gas insulated substation. In Proceedings of the 1st International Conference and Exhibition on Transmission and Distribution in the Asia Pacific Region, Yokohama, Japan, 6–10 October 2002; pp. 1220–1225.

20. Hosseinabadi, M.B.; Khanjani, N.; Ebrahimi, M.H.; Biganeh, J. Estimation of thermal power plant workers exposure to magnetic fields and simulation of hazard zones. *Radiat. Prot. Dosim.* **2020**, *190*, 289–296. [CrossRef]

21. Medved, D.; Zvanda, P. Electromagnetic Field Distribution Modeling and Measuring of the 110 kV Substation. In Proceedings of the 10th International Scientific Symposium on Electrical Power Engineering (ELEKTROENERGETIKA), Stara Lesna, Slovakia, 16–18 September 2019; pp. 81–86.

22. Roldán-Blay, C.; Roldán-Porta, C. Quick Calculation of Magnetic Flux Density in Electrical Facilities. *Appl. Sci.* **2020**, *10*, 891. [CrossRef]

23. Pirkkalainen, H.; Heiskanen, T.; Tonteri, J.; Elovaara, J.; Mika, P.; Korpinen, L. Measuring Occupational Exposure To Extremely Low-Frequency Electric Fields At 220 Kv Substations. *Radiat. Prot. Dosim.* **2017**, *176*, 400–403. [CrossRef]

24. Yang, J.M.; Zhang, W.F.; Zou, L.; Wang, Y.L.; Sun, Y.L.; Feng, Y.C. Research on Distribution and Shielding of Spatial Magnetic Field of a DC Air Core Smoothing Reactor. *Energies* **2019**, *12*, 937. [CrossRef]

25. Fontgalland, G.; de Andrade, H.D.; de Figueiredo, A.L.; Queiroz, I.D.; De Oliveira, A.H.S.; Paiva, J.L.S.; Sousa, M.E.T. Estimation of electric and magnetic fields in a 230 kV electrical substation using spatial interpolation techniques. *IET Sci. Meas. Technol.* **2021**, *15*, 411–418. [CrossRef]

26. Qiu, R.Q.; Zhu, F.; Yan, J.B.; Yu, K. Measurement and Analysis of Power Frequency Magnetic Field in Substation of Jing-Shi Passenger Railway Line. In Proceedings of the 5th IEEE International Symposium on Microwave, Antenna, Propagation and EMC Technologies for Wireless Communications (MAPE), Chengdu, China, 29–31 October 2013; pp. 582–585.

27. Okrainskaya, I.S.; Gladyshev, S.P.; Sidorov, A.I. Investigation of the Magnetic Field Intensity near the Equipment of the 500 kV Power Substation. In Proceedings of the IEEE International Conference on Electro/Information Technology (Eit), Dekalb, IL, USA, 21–23 May 2015; pp. 184–187.

28. Liu, B.; Ouyang, Z.Q.; Li, P.; Qu, Y.Y.; Wu, T.; Wei, Z. Study on magnetic field distribution of 10 kV switchgear and shielding efficiency of enclosure. In Proceedings of the 22nd International Conference on Electrical Machines and Systems (ICEMS), Harbin, China, 11–14 August 2019; pp. 1194–1198.

29. Tognola, G.; Chiaramello, E.; Bonato, M.; Magne, I.; Souques, M.; Fiocchi, S.; Parazzini, M.; Ravazzani, P. Cluster Analysis of Residential Personal Exposure to ELF Magnetic Field in Children: Effect of Environmental Variables. *Int. J. Environ. Res. Public Health* **2019**, *16*, 4363. [CrossRef] [PubMed]

30. Frigura-Iliasa, M.; Baloi, F.I.; Frigura-Iliasa, F.M.; Simo, A.; Musuroi, S.; Andea, P. Health-Related Electromagnetic Field Assessment in the Proximity of High Voltage Power Equipment. *Appl. Sci.* **2020**, *10*, 260. [CrossRef]

31. Malkowski, S.; Adhikari, R.; Hona, B.; Mattie, C.; Woods, D.; Yan, H.; Plaster, B. Technique for high axial shielding factor performance of large-scale, thin, open-ended, cylindrical Metglas magnetic shields. *Rev. Sci. Instrum.* **2011**, *82*, 075104. [CrossRef]